ACS OMEGA

Open Access

http://pubs.acs.org/journal/acsodf

Article

OSDA-Free Seeded Cu-Containing ZSM-5 Applied for NH_3–SCR-$DeNO_x$

Magdalena Jabłońska,* Ana Palčić, Muhammad Fernadi Lukman, Anna Wach, Marko Bertmer, David Poppitz, Reinhard Denecke, Xiaochao Wu, Ulrich Simon, Andreas Pöppl, and Roger Gläser

Cite This: *ACS Omega* 2023, 8, 41107–41119

Read Online

ACCESS | Metrics & More | Article Recommendations | Supporting Information

ABSTRACT: A series of ZSM-5 zeolite materials were synthesized from organic structure-directing agent (OSDA)-free seeded systems, including nanosized silicalite-1 (12 wt % water suspension or in powder form) or nanosized ZSM-5 (powder form of ZSM-5 prepared at 100 or 170 °C). The physicochemical characterization revealed aggregated species in the samples based on silicalite-1. Contrarily, the catalysts based on ZSM-5 seeds revealed isolated copper species, and thus, higher NO conversion during the selective catalytic reduction of NO_x with NH_3 (NH_3–SCR-$DeNO_x$) was observed. Furthermore, a comparison of the Cu-containing ZSM-5 catalysts, conventionally prepared in the presence of OSDAs and prepared with an environmentally more benign approach (without OSDAs), revealed their comparable activity in NH_3–SCR-$DeNO_x$.

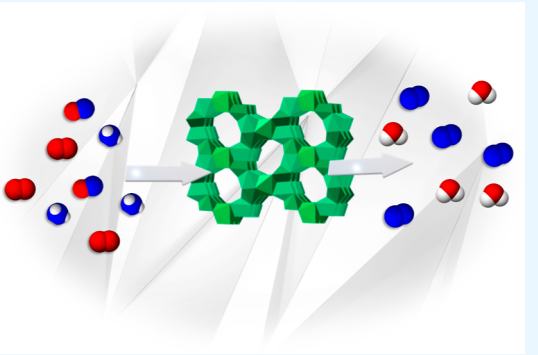

1. INTRODUCTION

In line with current tendencies that aspire to render the existing industrial processes as well as everyday human actions, practices, and habits more environmentally friendly, sustainable, and equitable, the scientists in academia and industry work on ameliorating these activities as well as developing new ones. In chemistry and material science in general, this assumes an increased yield of prepared materials employing as little as possible of potentially harmful chemicals, e.g., organic solvents, under the conditions of lowest possible energy consumption. Zeolites are a class of porous materials that are widely used in all fields of human activities, from large industrial facilities to households.[1] In addition, new usage options are continuously investigated.[2] Hence, there is great interest in carrying out their production in accordance with ecological requirements. Zeolite synthesis involving seed crystals in the system represents one of the possible avenues to address this issue. Seeds facilitate the formation of zeolites by reducing the synthesis period, governing the phase composition of the prepared material, and hampering the formation of side products. Often these reactions take place without the presence of organic structure-directing agents (OSDAs), making them environmentally acceptable processes.[3] In some cases, merely a catalytic quantity of seeds in the system induces the preparation of the target zeolite.[4] Previous findings demonstrate that the amount and the size of the added seeds affect the size and the morphology of the product by directing the crystal growth processes.[5] In the OSDA-free synthesis of ZSM-5, two approaches are commonly applied, including the template-free direct synthesis strategy (in which an aluminosilicate gel is heated to directly produce ZSM-5) or the seed-assisted template-free method (in which the silicate units are directed to form the MFI structure using seeds added to the aluminosilicate synthesis mixture).[6] In previously conducted studies, not only ZSM-5 but also ZSM-8, ZSM-11, and silicalite-1 zeolite materials have been applied as crystalline seeds for the synthesis of ZSM-5.[7−10]

Cu-ZSM-5 materials are investigated for their activity and N_2 selectivity in NH_3–SCR-$DeNO_x$ or the selective catalytic oxidation of ammonia into nitrogen and water vapor (NH_3–SCO). Our earlier study[11] showed that the Cu-ZSM-5 catalyst (among Cu-TNU-9, Cu-FER, and Cu–Y) displays an extraordinary activity in NH_3–SCR-$DeNO_x$, achieving 100% conversion at 175 °C with almost 100% selectivity for the formation of N_2. Furthermore, the results of the catalytic data revealed that the microporous structure was necessary for the formation of isolated Cu^+/Cu^{2+} species,[12] while the n(Si)/n(Al) ratio governs the copper site speciation. The variation in the framework n(Si)/n(Al) ratio of 19.8–50.5 was achieved via changes in the zeolite preparation temperature from 100 to 170 °C. The results of catalytic studies demonstrate that the ZSM-5 materials synthesized at a higher temperature, i.e., 170 °C, and thus a lower n(Si)/n(Al) ratio, exhibit more than 80%

Received: May 26, 2023
Accepted: September 6, 2023
Published: October 24, 2023

NO conversion between 175 and 450 °C. Other studied ZSM-5 zeolite catalysts were significantly less active, due to the presence of aggregated copper species.[13] Thus, Cu-ZSM-5 is deemed as a promising NH_3−SCR-DeNO_x catalyst; so in the follow-up studies, we applied a series of MFI-type zeolite seeds for the preparation of ZSM-5 zeolite materials and subsequently their Cu-forms by ion exchange. The seed-assisted OSDA-free preparation approach has been exploited as it potentially could provide a more environmentally friendly means to obtain an efficient NH_3−SCR-DeNO_x catalyst. Zeolite synthesis avenue from OSDA-free reaction mixture with added seeds enabled the preparation of a range of industrially relevant zeolites such as beta,[14] MOR, and MFI.[15] However, most of them were not tested as catalysts in the NH_3−SCR-DeNO_x reaction, so the evaluation of the performance of zeolites derived from OSDA-free seed-assisted systems under such conditions is indispensable. The Cu-containing zeolites were characterized in terms of their structure and morphology (XRD, SEM, TEM, ICP-OES, XPS, and NMR), texture (N_2 sorption), acidity (FT-IR studies of NH_3 sorption), and the nature of the copper species (DR UV−vis, TPR-H_2, TEM, XAS, and EPR). In order to determine the effect of the usage of different seeds in the preparation of Cu-containing ZSM-5 on the catalytic activity, the catalysts were investigated for the NH_3−SCR-DeNO_x reaction. Although Cu-containing ZSM-5 catalysts were examined for their high-temperature stability,[16,17] we did not focus our studies on this topic. Otherwise, the respective time-on-stream catalytic results are provided.

2. EXPERIMENTAL SECTION

2.1. Catalyst Preparation. Nanosized silicalite-1 seeds were prepared from a reaction mixture having the following molar oxide composition: 4.5 $(TPA)_2O$: 25 SiO_2: 480 H_2O: 100 EtOH according to the previously published procedure using appropriate amounts of tetraethylorthosilicate (TEOS, Aldrich, 98 wt %), tetrapropylammonium hydroxide (TPAOH, 20 wt % in water, Alfa Aesar), and doubly distilled water produced in our laboratory.[18] After mixing the reactants, the synthesis mixture was hydrolyzed overnight and hydrothermally treated at 60 °C for 3 weeks. Upon synthesis, the solid product was washed with distilled water using a high-speed centrifuge until the pH of the supernatant reached the value of 7. Afterward, silicalite-1 suspensions having 12 wt % seed content were prepared, and a part of the suspension was freeze-dried to recover a solid material that was employed as seeds in the form of powder. Nanosized ZSM-5 seeds were prepared from a reaction mixture of the following molar oxide composition: 1.23 Na_2O: 9.74 TPAOH: 1.0 Al_2O_3: 43.2 SiO_2: 806 H_2O according to the previously published procedure using appropriate amounts of sodium aluminate [$NaAlO_2$, Riedel de Haën, $w(Al_2O_3)$ = 54 wt %, $w(Na_2O)$ = 41 wt %], TPAOH (Alfa Aesar, 20 wt % in water), and double distilled water.[19] Upon obtaining a clear mixture by stirring, TEOS (Aldrich, 98 wt %) was admixed to the solution and hydrolyzed at 80 °C for 24 h. The synthesis was conducted at 100 °C for 7 days and at 170 °C for 5 days. Collected solid phases were washed with distilled water using a high-speed centrifuge until the pH of the suspension reached the value of 7. The washed samples were freeze-dried to obtain seeds in the form of powder.

The OSDA-free seeded synthesis of nanosized ZSM-5 materials was performed from synthesis mixtures having the molar oxide composition of 7.4 Na_2O: 0.88 Al_2O_3: 25 SiO_2: 1168 H_2O according to the modified procedure of Majano et al.[5] An appropriate amount of water glass sodium silicate [sodium silicate solution, Honeywell, reagent grade, w(NaOH) = 14 wt %, $w(SiO_2)$ = 27 wt %], doubly distilled water, and seeds were stirred for 20 min. Precursor gels containing 15 wt % of seeds with respect to the silica content were prepared. The alumina component was prepared by dissolving $Al_2(SO_4)_3{\cdot}18H_2O$ (p.a., Kemika, 98 wt %) in water and subsequently mixed into the silicon component under vigorous stirring. Silicalite-1 seeds were added as a 12 wt % water suspension (the final product label was Cu-ZSM-5_1) or as a dry noncalcined powder (the final product label was Cu-ZSM-5_2). The powder was easier to store and handle. ZSM-5 seeds prepared at 100 and 170 °C were added as a noncalcined powder (the final product labels were Cu-ZSM-5_3 and Cu-ZSM-5_4, respectively). In the case when silicalite-1 seeds were added in the form of a suspension, the amount of water in the suspension was compensated for by the addition of less water to the silicate solution. The crystallization was performed at 180 °C (as indicated from the reference studies[20−22] that served as the basis for this seeded synthesis) for 12 days. After hydrothermal transformation, the end product was washed until a neutral pH value was obtained, dried at 105 °C, and afterward calcined in air at 550 °C for 5 h (heating rate 1.75 °C min^{-1}).

The calcined samples were subjected to the ion-exchange procedure with 0.5 M aqueous solution of ammonium chloride (p.a., Kemika, 98 wt %) at 80 °C for 3 h. Three consecutive exchange steps were carried out followed by calcination in static air at 550 °C for 5 h (heating rate 1.75 °C min^{-1}) in order to prepare zeolites in the proton form. These materials were further ion-exchanged with 0.05 M solution of copper(II) acetate (p.a., Kemika, 98 wt %) at room temperature for 24 h. Finally, the Cu-ZSM-5 materials were calcined at 550 °C for 4 h.

2.2. Catalyst Characterization. The hydrodynamic diameters in the suspension of seed crystals were evaluated by using a Malvern Zetasizer Nano (Malvern, UK) instrument. Dynamic light scattering (DLS) analysis was performed under a scattering angle of 173° by employing a HeNe laser with 3 mW output power at a wavelength of 632.8 nm.

The X-ray diffraction (XRD) powder patterns of the studied materials were recorded using a HUBER G670 (Rimsting, Germany) diffractometer applying CuKα radiation with a wavelength of 0.154 nm. Data were collected with a scanning range of the diffraction angle 2θ between 5 and 60° in intervals of 0.005°.

Analysis of the chemical composition of the samples (i.e., Al, Si, or Cu content) was carried out by inductively coupled plasma optical emission spectroscopy (ICP-OES) using a PerkinElmer Optima 8000 instrument (Rodgau, Germany). The solid samples (approximately 20 mg) were dissolved in a mixture of HF (2 mL, 47−51 wt %, Sigma-Aldrich), HNO_3 (3 mL, 69 wt %, Sigma-Aldrich), and HCl (3 mL, 35 wt %, Sigma-Aldrich), and the mixture was irradiated with microwaves (1 h, 200 °C). Before measurement, HF was removed by complexing with H_3BO_3 (12 mL, 99.99 wt %, Sigma-Aldrich) under microwave radiation (5 min, 200 °C).

X-ray photoelectron spectroscopy (XPS) spectra were recorded using a Focus CSA-150 electron energy analyzer (Hünstetten-Kesselbach, Germany) with a pass energy of 100 eV resulting in an overall resolution of about 2 eV. Excitation

https://doi.org/10.1021/acsomega.3c03721
ACS Omega 2023, 8, 41107−41119

was supplied by nonmonochromatized Al and Mg Kα rays. The samples were pressed as pellets and mounted with tantalum stripes, while heating steps were performed by using a filament heater. Data analysis has been performed using the UNIFIT software.[23]

Nitrogen physisorption was conducted at −196 °C using a MicrotracBEL Corp., BELSORP-miniX (Haan/Duesseldorf, Germany). Prior to analysis, each sample (ca. 100−200 mg) was activated at 250 °C and 1 Pa. The Brunauer−Emmett−Teller (BET) method was used for the determination of the specific surface area. The pore width distribution was obtained from the desorption branch of the nitrogen sorption isotherm using the Barrett−Joyner−Halenda (BJH) method. The total pore volume was taken from the isotherm point at $p{\cdot}p_0^{-1}$ = 0.99. The micropore volume and the specific surface area of micropores were calculated using the Harkins and Jura model (t-plot analysis, thickness range of 0.58−1.20 nm).

Scanning electron microscopy (SEM) analysis was performed using a ZEISS LEO Gemini 1530 (Oberkochen, Germany) microscope operated at an acceleration voltage of 10 kV, working distance of about 6 mm, and aperture size of 30 μm. The samples were placed on conductive carbon pads and sputtered with gold for conductivity.

Transmission electron microscopy (TEM) analysis was carried out using a JEM-2100Plus instrument from JEOL (Tokyo, Japan) operated at an accelerating voltage of 200 kV and equipped with a LaB_6 cathode as well as a high-resolution pole piece. The images were recorded with a TVIPS 4K CMOS camera system (Gauting, Germany). The samples were ground in ethanol, and the dispersed particles were supported on a holey carbon on a Ni-TEM grid.

Diffuse reflectance (DR) UV−vis spectra of the samples were measured under ambient conditions with a PerkinElmer LAMBDA 650S UV−vis spectrometer (Rodgau, Germany) equipped with a 150 mm integrating sphere. As a reference material, a Spectralon (PTFE, reflective value 99%, Rodgau, Germany) was used. The experiments were carried out in the wavelength range of 200−900 nm (step width of 1 nm; slit width of 2 nm).

The profiles of temperature-programed reduction of the samples with hydrogen (TPR-H_2) were obtained using a MicrotracBEL BELCAT II analyzer (Osaka, Japan). Prior to the TPR-H_2 experiment, the sample (50 mg) was heated from room temperature to 300 °C for 0.5 h (with a heating rate of 10 °C min^{-1} in a 20 vol % O_2 diluted in Ar with a total flow of 6 mL min^{-1}). After cooling down (to 100 °C under pure Ar with a total flow of 20 mL min^{-1}), the sample was reduced in the temperature range between 100 and 800 °C (with 5 vol % H_2 diluted in Ar, and a heating ramp of 10 °C min^{-1} at a total flow rate of 30 mL min^{-1}). A thermal conductivity detector (TCD) was applied to measure the H_2 consumption, while pulse calibration of the TCD was performed for every single experiment.

X-ray absorption spectroscopy (XAS) measurements were performed at the SuperXAS beamline of the Swiss Light Source (SLS) of the Paul Scherrer Institute (Villigen, Switzerland). The incident photon beam from the storage ring was collimated by a Si-coated mirror, followed by monochromatization by a liquid-cooled Si(111) channel-cut crystal. The measurements were performed in QEXAFS mode, which allowed for rapid collection of Cu K-edge XAS spectra in transmission mode (300 s/sample). Copper-containing zeolites were pressed in 10 mm diameter pellets, using optimal amounts for transmission measurements, and homogeneously mixed with cellulose. The spectra of the Cu foil were collected simultaneously for internal energy calibration (edge energy, E_0 = 8979 eV). The resulting raw data were preprocessed using the in-house developed ProQEXAFS software.[24] Standard XAS data reduction steps (i.e., subtraction of pre-edge and post-edge backgrounds, determination of the edge energy, and normalization of the data set to an edge jump of 1) were performed with Athena software.[25]

The electron paramagnetic resonance (EPR) study was conducted with a Bruker EMX micro (X-band, 9.4 GHz, Rheinstetten, Germany) spectrometer fitted with an ER 4119 HS resonator. Low-temperature measurements were realized using an Oxford Instruments He cryostat ESR 900. During data analysis, the EPR spectral simulations were performed using the MATLAB-based simulation package EasySpin.[26] The microwave power was adjusted so that no line shape distortion could occur, whereas the modulation amplitude was set to 1 mT. Powder samples (ca. 20 mg) were put into an EPR quartz glass with a 3.8 mm inner diameter and then sealed to avoid contact with air. Prior to the experiment, the sample was activated at 400 °C for 5 h under vacuum conditions (i.e., 10^{-4}−10^{-5} Pa).

Solid-state NMR measurements were performed with a 17.6 T magnet and a Bruker AVANCE spectrometer (Rheinstetten, Germany) by using a 4 mm MAS probe. ^{27}Al spectra (195 MHz) were obtained after a single 1 μs pulse with a short flip angle at a spinning frequency of 12 kHz. ^{29}Si measurements (148.7 MHz) were done either with direct excitation (90° pulse length of 2.5 μs) and a recycle delay of 5 s or using cross-polarization with a contact time of 5 ms and a recycle delay of 1 s. In both cases, the spinning frequency was 7 kHz. Spectra were referenced to a 1 M solution of $Al(NO_3)_3$ and TMS for ^{27}Al and ^{29}Si, respectively. Deconvolution of the spectra was done with the program dmfit.[27]

In situ diffuse reflectance infrared Fourier transform spectroscopy (DRIFTS) was carried out using an FT-IR VERTEX 70 device (Bruker, Germany) and an accessory Harrick Praying Mantis mirror system. The samples were placed inside a high-temperature reaction chamber (HVC−DRP, Harrick Scientific Products, Inc.) and heated to 350 °C for 1.5 h in a flow of pure N_2 (with a flow rate of 120 mL min^{-1}). Subsequently, the chamber with the sample was cooled down and kept at 150 °C. The spectrum collected in flowing N_2 was used as background and was subtracted from the spectra collected afterward. Then, a flow of 575 ppm of NH_3 and balance N_2 (total flow of 120 mL min^{-1}) was fed onto the catalyst surface and held for 0.5 h; afterward, the spectra were collected.

2.3. Catalytic Experiments. The catalytic experiments were carried out in a fixed-bed quartz tube reactor [inner diameter (ID): 6 mm; length (L): 200 mm] at atmospheric pressure. Prior to each experiment, the catalyst (100 mg, a fraction of particle size in the range of 200−400 μm) was activated at 350 °C for 1.5 h under a flow of pure He (50 mL min^{-1}). After cooling down to ca. 50 °C, the simulated flue gas, composed of 0.05 vol % NO, 0.0575 vol % NH_3 and 4 vol % O_2, 5 vol % H_2O, and balance He (with a total flow rate of 120 mL min^{-1}) or 0.1 vol % NO, 0.1 vol % NH_3, and 10 vol % O_2 diluted in He (with a total flow rate of 120 mL min^{-1}), was switched on to pass through the catalyst bed. The gas hourly space velocity (GHSV) was set to be ∼30,000 h^{-1}. The reaction was carried out in the temperature range from 50 to

https://doi.org/10.1021/acsomega.3c03721
ACS Omega 2023, 8, 41107−41119

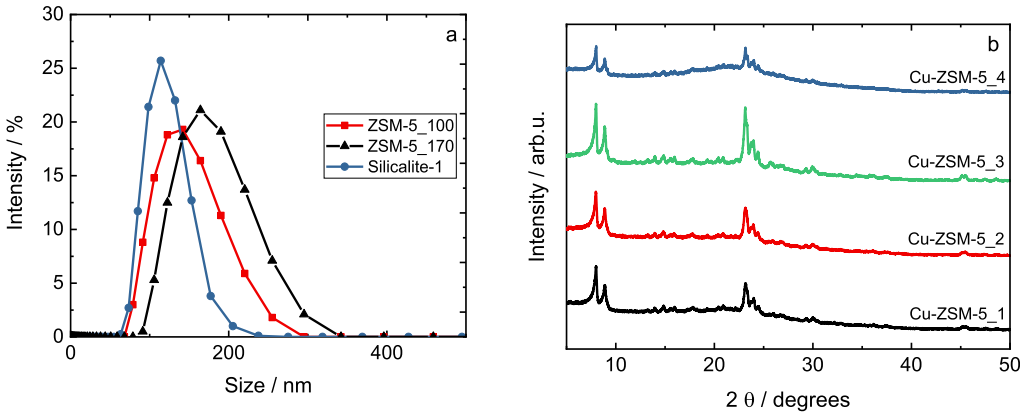

Figure 1. (a) Particle size distribution obtained by DLS for the different seed crystals, and (b) XRD patterns of Cu-containing ZSM-5 materials prepared by seeding (sample labels as in Table 1).

Table 1. Results of the Elemental Analysis by ICP-OES of the Cu-Containing ZSM-5, ω_i: Mass Fractions[a]

sample	ω_{Al}/wt %	ω_{Si}/wt %	ω_{Cu}/wt %	ω_{Na}/wt %	n(Si)/n(Al)		n(Cu)/n(Al)	
					ICP	XPS	ICP	XPS
Cu-ZSM-5_1	6.9	32.4	1.7	1.1	4.5	5.8	0.1	0.1
Cu-ZSM-5_2	4.3	34.8	2.0	0.1	7.8	4.9	0.2	0.1
Cu-ZSM-5_3	4.5	35.7	2.6	0.1	7.6	5.0	0.3	0.2
Cu-ZSM-5_4	5.3	33.0	2.3	0.3	6.0	6.1	0.2	0.1

[a]Atomic ratios as determined by ICP-OES and XPS.

450 °C with an interval of 25−50 °C. At each temperature, the reaction was stabilized for 70−90 min before quantitative analysis of the NO concentration. The gas leaving the reactor was washed in a gas-washing bottle filled with concentrated phosphoric acid. The NO and NO_x concentrations were continuously monitored using a CLD 70 S Chemiluminescence Analyzer (Tutzing, Germany). The conversion of NO (X(NO)) was determined according to the following equation $X(NO) = ([c(NO)_{in} - c(NO)_{out}]/c(NO)_{in}) \times 100\%$, where $c(NO)_{in}$ and $c(NO)_{out}$ refer to the concentration of NO in the inlet and the outlet gas, respectively. The experimental uncertainty of the calculated NO conversion was found to be ±2% (as indicated by repeated measurements of identical catalysts).

The turnover frequency (TOF) values for Cu-containing zeolites during NH_3−SCR-DeNO_x were calculated using the following equation: TOF (s^{-1}) = (c(NO) × X(NO) × F)/(m/m_W), where c(NO), X(NO), and F are the concentration of NO (mol mL^{-1}), NO conversion (%), volumetric flow rate (mL s^{-1}), respectively. Also, m and m_W are the copper loading (g) on the catalyst and the molecular weight (63.54 g mol^{-1}) of copper, respectively.

The standard reaction on Cu-containing zeolites can be considered as a first-order reaction with respect to NO. According to the first-order power-law equation: $-R_{SCR} = k_a \times c$(NO), in which, k_a (mL g^{-1} s^{-1}) represents the apparent rate constant. The correlation between k_a and NO conversion (X(NO)) is expressed as follows: $k_a = -(F/(c(NO) \times W))\ln(1 - X(NO))$, where F (mol s^{-1}) is the molar NO feed rate, c(NO) (mol mL^{-1}) is the concentration of NO, W (g) is the catalyst amount, and X(NO) is NO conversion (%).[28] The apparent activation energy (E_a) was calculated from the slope of linear regression derived from the Arrhenius equation $k_a = A \cdot \exp(-E_a\ R^{-1}\ T^{-1})$. To minimize the influence of heat generated from the exothermic reaction as well as the mass transfer issue, the measurements and following calculations were performed for data points with a conversion lower than 25% (in the three-point linear regression model).

3. RESULTS AND DISCUSSION

In the scope of this study, the MFI-type zeolite materials (ZSM-5) were prepared via the addition of nanosized seed crystals to the OSDA-free reaction mixture that was subsequently hydrothermally treated at 180 °C. Three different kinds of seed crystals were used—silicalite-1 (all-silica material) and ZSM-5 materials (Al-counterpart of MFI-type material) prepared at 100 and 170 °C. The particle size distribution measured by DLS, displayed in Figure 1a, reveals that in all seed systems, the crystals are smaller than 350 nm. In silicalite-1, the size distribution spans from 70 to 220 nm, whereas for the ZSM-5 samples obtained at 100 and 170 °C, the ranges are 70−300 and 95−325 nm, respectively. The seed ZSM-5 crystals were added in the form of powder. For the sake of comparison, silicalite-1 seeds suspended in water were also employed. The values of the n(Si)/n(Al) ratio of the prepared Cu-ZSM-5 materials presented in Table 1 stretch from 4.5 to 7.8, which is lower than that of the initial synthesis gel (i.e., 16.3). It suggests that under the studied conditions, the solubility of silicate species is rather high with respect to the solubility of the aluminosilicate species, meaning that the materials possess either a high share of amorphous silica/alumina phases or other Al-rich phases in these samples. This effect is particularly pronounced in the case when silicalite-1 seeds were used in the form of a suspension and the lowest n(Si)/n(Al) ratio of 4.5 was attained. The data in Table 1 reveal that the presence of Al in the seed crystals does not further affect the chemical composition of the formed ZSM-5 materials. The n(Si)/n(Al) obtained from XPS analysis varied slightly (within the expected error bars) from the one measured via ICP-OES, indicating that the distribution of Al

https://doi.org/10.1021/acsomega.3c03721
ACS Omega 2023, 8, 41107−41119

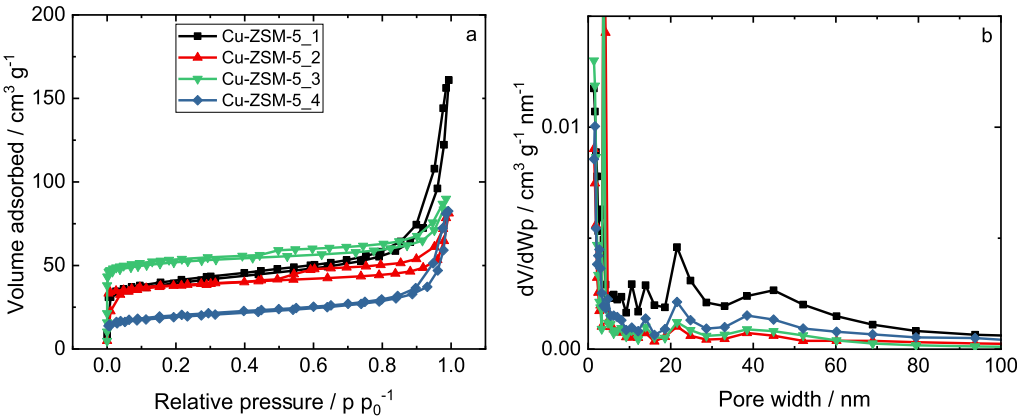

Figure 2. (a) N_2 sorption isotherms and (b) pore width distribution of Cu-containing ZSM-5; in (a,b), the sample labels are equal.

Table 2. Textural Properties of the Samples Determined from the N_2 Sorption Measurements: Specific Surface Area [A_S(BET)], Micropore Pore Volume (V_{MIC}), Mesopore Pore Volume (V_{MES}), and Total Pore Volume (V_{TOT})

sample	A_S(BET)/m^2 g^{-1}	V_{TOT}/cm^3 g^{-1}	$V_{(MIC)}$/cm^3 g^{-1}	$V_{(MES)}$/cm^3 g^{-1}
Cu-ZSM-5_1	129	0.23	0.06	0.17
Cu-ZSM-5_2	126	0.12	0.06	0.06
Cu-ZSM-5_3	170	0.14	0.08	0.06
Cu-ZSM-5_4	69	0.12	0.02	0.10

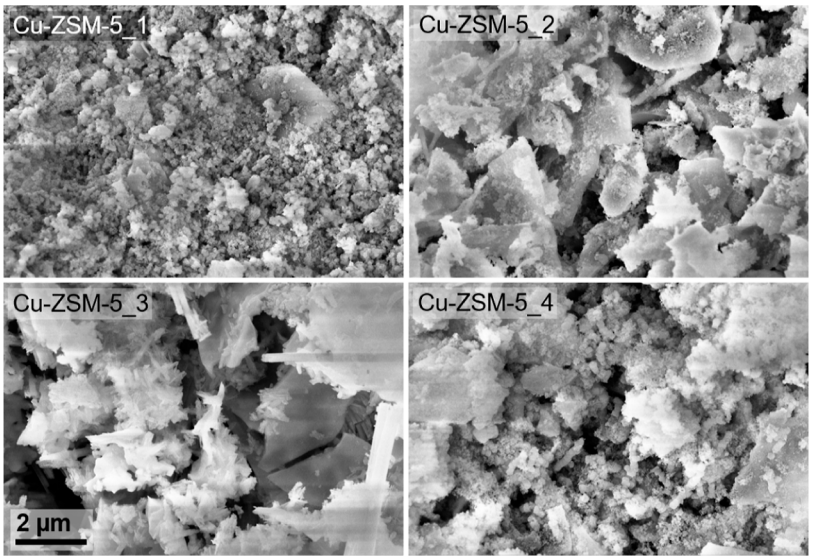

Figure 3. SEM micrographs of the studied series of Cu-containing ZSM-5 (scale markers refer to all images).

within the particles of the powder is not uniform. Figure SI1 shows the XRD patterns of the products of the respective syntheses before the Cu ion exchange. Diffraction peaks characteristic of MFI-type materials are clearly visible in all samples. The total intensity of the patterns as well as the pattern profile suggest that the ordering degree is the lowest in the sample ZSM-5_4 as it presents the least resolved peaks. The XRD patterns of the Cu-modified samples depicted in Figure 1b indicate retention of the zeolite framework upon ion exchange. Still, in all samples, a certain amount of the amorphous phase was detected. Here, too, the profile and intensity of the patterns of sample Cu-ZSM-5_4 indicate the lowest fraction of crystalline matter.

Nitrogen sorption data (Figure 2a, Table 2) corroborate this conclusion as the micropore volume is lower compared to those of highly crystalline MFI-type zeolite materials reported in the literature.[18,29] Indeed, the absence of the organic structure-directing agent in the preparation system could render the crystallization process incomplete, leading to a lower crystallization degree. The specific surface area of Cu-ZSM-5_4 is in line with the lowest crystallinity of this sample. Nevertheless, all samples exhibit a combination of type I and type IVa N_2 sorption isotherms with H4 hysteresis loops that begin to develop at $p{\cdot}p_0^{-1} > 0.8$. The measured profile is typical for aggregated nanoparticles.[30,31] This conclusion is in line with the SEM study (Figure 3) in which large aggregates composed of small particles are observed in all samples. Furthermore, in all samples, several amorphous particles are visible in accordance with the XRD and N_2 sorption data. In the samples Cu-ZSM-5_1, Cu-ZSM-5_2, and Cu-ZSM-5_4, the small constituent particles present a spherical morphology, whereas in the sample Cu-ZSM-5_3, they are needle-like

https://doi.org/10.1021/acsomega.3c03721
ACS Omega 2023, 8, 41107−41119

(elongated with sharp edges). The reason could be the difference in the solubility of Si species and its high tendency for polymerization/precipitation. The size of the constituent particles varies between the samples, which, together with different morphologies, indicates differences in the crystal growth process in the studied systems. The smallest constituent particles are found in the system with previously suspended silicalite-1 crystals. Taking into consideration that the amount of the seed crystals is equal in all systems, clearly, the properties and the admission form of the seed crystals influence the zeolite formation processes and govern the features of the product. However, establishing the precise relationship between the properties of the seeds and the zeolite crystallization mechanism is out of the scope of this study.

TEM imaging (Figure 4, left) shows the presence of crystals as well as amorphous material. Similarly, as observed in SEM analysis, the constituent MFI crystals in each sample differ in size and morphology, which once again suggests divergent crystal growth processes in zeolite synthesis mixtures having various forms of seeds. Moreover, amorphous material has been observed in each sample in accordance with XRD and N_2 findings. However, the size and shape of these amorphous particles are rather inhomogeneous too. Consequently, no correlation or trend to crystal growth parameters could be established from TEM imaging. Furthermore, Cu nanoparticles smaller than 5 nm were found in all samples by TEM high-resolution imaging (Figure 4, right). These nanoparticles are evenly distributed and found in both the crystallites and amorphous particles, and no significant differences between the samples could be identified.

Figure 5 displays the ^{29}Si and ^{27}Al NMR spectra. All samples show comparable spectra. ^{29}Si spectra are characterized by a dominant, broad signal at −107 ppm representing a superposition of resonances arising due to the Q^3 Si species ((HO)−Si-[$(OSi)_3$]) and ([$(OSi)_3$]-Si-[OAl]).[32] Its amount is fairly constant among samples Cu-ZSM-5_1 to Cu-ZSM-5_3 but significantly higher for sample Cu-ZSM-5_4, which indicates the lowest level of ordering. This finding could explain the lowest value of the micropore volume for this particular sample. Additionally, two signals at −112 and −115 ppm represent Q^4 Si atoms (-Si-[$(OSi)_4$]). A typical spectral deconvolution is given in Figure SI2a; the quantitative deconvolution is summarized in Table SI1. In the ^{29}Si{^{1}H} CPMAS spectra, the −107 ppm signal is clearly enhanced due to the close connectivity to hydrogen, meaning there are Q^3 silanol point defects in all of the samples.

The ^{27}Al MAS NMR spectra are all characterized by three signals with isotropic chemical shifts of 57, 39, and 6 ppm attributed to four-, five-, and six-coordinated aluminum sites. A typical deconvolution and the relative amounts of the three sites are included in Figure SI2b and Table SI2. The relative amounts vary only minorly between the four samples, with sample Cu-ZSM-5_4 showing lower five- and higher six-coordinated aluminum contents. Therefore, conducting the ZSM-5 synthesis in an OSDA-free reaction system seems to render the process incomplete, leading to materials with displaced or even partially detached aluminum from the zeolite framework.

Figure 6a shows the DR UV−vis spectra of Cu-containing ZSM-5. The band in the 200−260 nm range is associated with ligand-to-metal charge transfer from oxygen in the zeolitic framework to isolated copper ions. The band above 550 nm originates from d−d transitions of distorted octahedral aqua

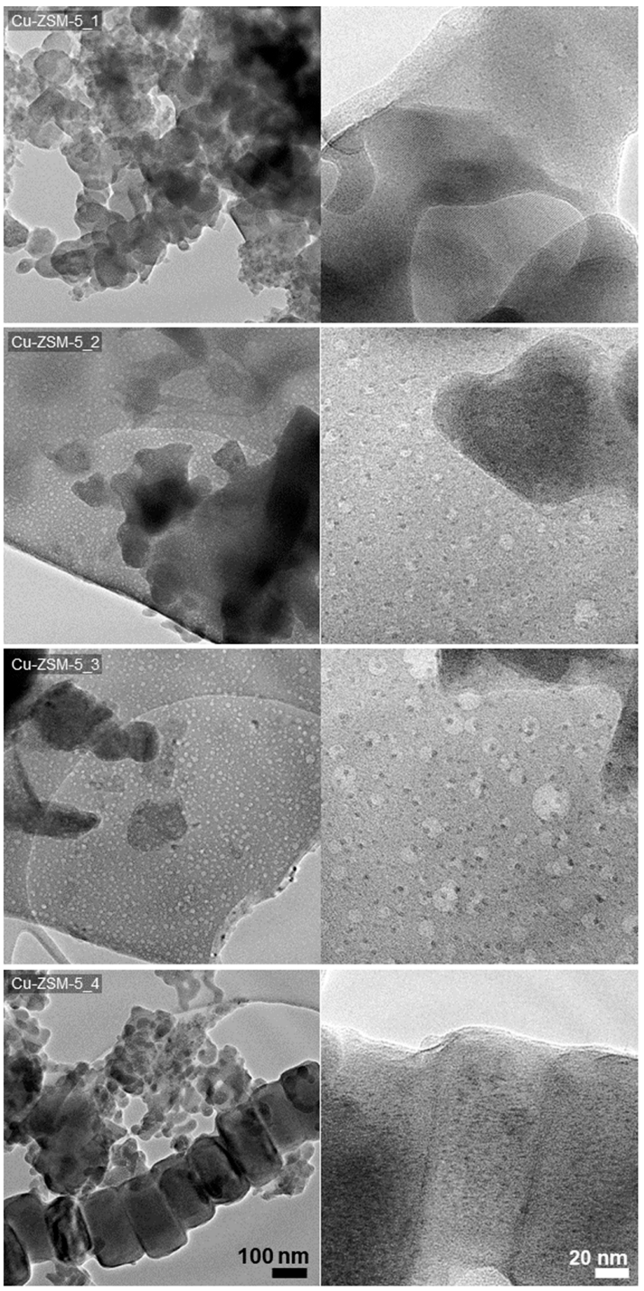

Figure 4. TEM overview images (left) and corresponding high-resolution images (right) of the Cu-containing ZSM-5. The scale bar is identical for all images on the left or right side.

complexes of isolated Cu^{2+}, which are typically found in hydrated Cu-containing zeolitic materials. The bands in the range of 260−550 nm proved the presence of the CuO species and the $[Cu-O-Cu]^{2+}$ species.[11−13] Clearly, Cu-ZSM-5_3 and Cu-ZSM-5_4 possess isolated copper species. Cu-ZSM-5_1 (based on silicalite-1 seeds that were added as 12 wt % water suspension) possesses the lowest amount of cation exchange sites. Contrarily, the materials based on silicalite-1 revealed aggregated copper species, which is further confirmed by TPR-H_2. Figure 6b shows the TPR-H_2 profiles of Cu-containing ZSM-5. According to literature indications,[13,33−35] the reduction profile of Cu-containing ZSM-5 consists of three reduction steps attributed to $Cu^{2+} \rightarrow Cu^{+}$, $CuO \rightarrow Cu^{0}$ (below 300 °C), and $Cu^{+} \rightarrow Cu^{0}$ (above 300 °C). These steps can be

https://doi.org/10.1021/acsomega.3c03721
ACS Omega 2023, 8, 41107−41119

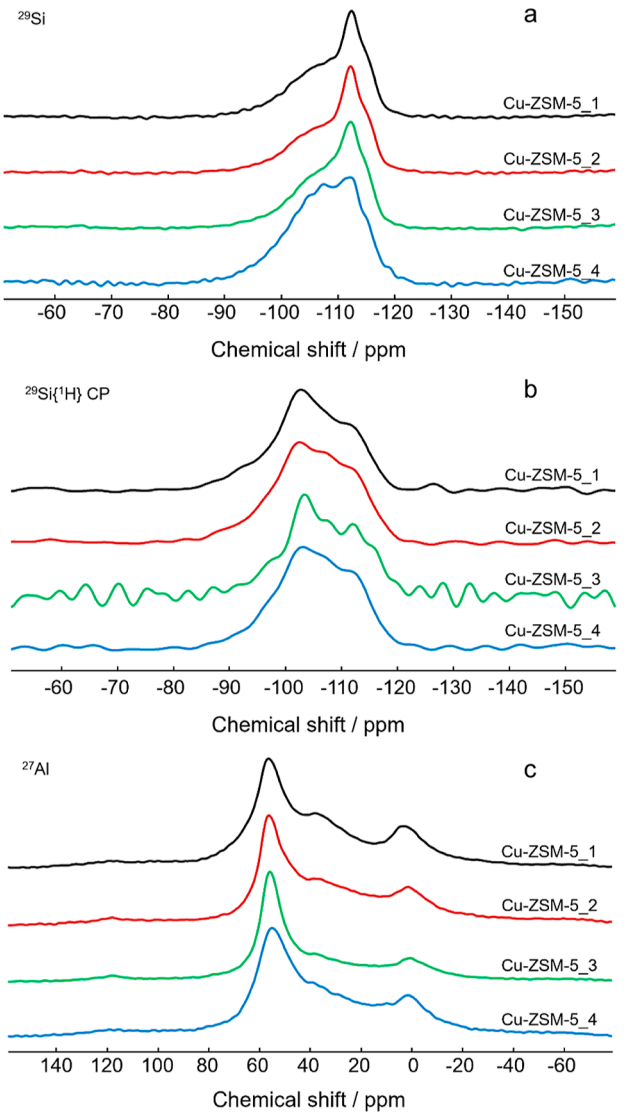

Figure 5. (a) ^{29}Si Bloch decay, (b) ^{29}Si{^{1}H} CP, and (c) ^{27}Al MAS NMR spectra of Cu-containing ZSM-5.

identified in the profile of the samples; however, the reduction temperatures varied significantly among them, indicating altered reducibility of the involved copper species (Cu^{2+} → Cu^{+}: below 300 °C, CuO → Cu^{0}: ca. 300−400 °C, and Cu^{+} → Cu^{0}: above 400 °C). Cu-ZSM-5_1 possessing the lowest amount of copper species (1.7 wt %, Table 1) also reveals the highest amount of CuO species, indicating that copper species existed mainly on the surface of this material. Furthermore, the broad reduction bands above 450 °C recorded for this material appear due to water evolution,[36] in agreement with DR UV−vis analysis. The water evolution during TPR-H_2 in this region cannot also be excluded in the case of other samples.

To elucidate the nature of the copper species, all Cu-containing zeolites prepared from OSDA-free systems with different seeds were investigated by X-ray absorption near-edge spectroscopy (XANES). The XANES spectra are the fingerprint of the local atomic and electronic structures around the absorbing atom, a powerful tool for the characterization of the local atomic structure.[37] The normalized XANES spectra collected at the Cu K-edge for Cu-ZSM-5, along with Cu reference compounds [CuO and $Cu(OH)_2$] are compared in Figure 7. The discussion about other reference materials was

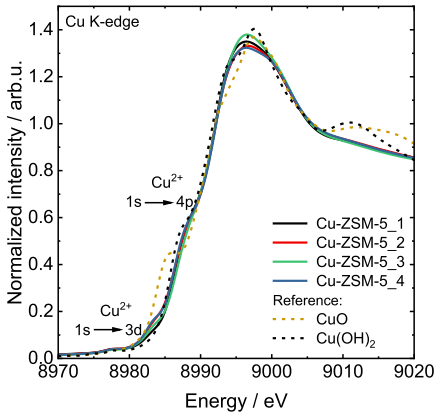

Figure 7. Normalized Cu K-edge XANES spectra of Cu-containing ZSM-5.

already published in the previous paper.[38] The copper species located in zeolites have a very complex nature, and they cannot be easily compared to the standard reference materials. In all presented spectra in these studies, a weak pre-edge feature is observed at 8977.8 eV, indicating a Cu^{2+} state. This feature is attributed to 1s → 3d transitions, which is formally dipole-forbidden but gains intensity through 3d−4p mixing and direct quadrupole coupling.[39,40] It is noteworthy that the pre-edge is dependent on the number of metal 3d holes and therefore is not observed in d^{10} systems, such as Cu^{0} and Cu^{+} species, due to fully filled d-orbitals. In all copper-containing ZSM-5

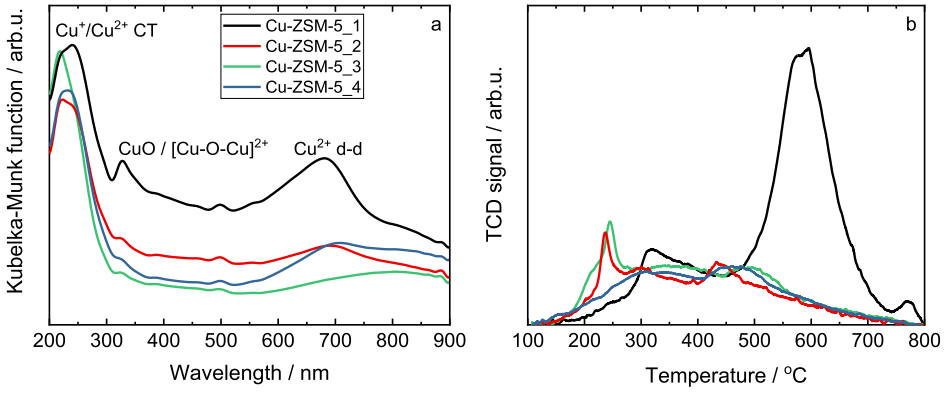

Figure 6. (a) DR UV−vis spectra and (b) TPR-H_2 profiles of Cu-containing ZSM-5; in (a,b), the sample labels are equal.

https://doi.org/10.1021/acsomega.3c03721
ACS Omega 2023, 8, 41107−41119

zeolites, the edge energy position (defined at the first inflection point on the rising absorption edge), located at 8986.4 ± 0.2 eV, corresponds to dipole-allowed Cu^{2+} 1s → 4p transitions. In addition, a high-intensity white line is observed at ca. 8996.4 eV, which is characteristic of Cu^{2+} species in a highly coordinated form, with a combination of water, framework oxygen, and OH groups in the coordination sphere. The collected XANES spectra of the as-prepared Cu-containing ZSM-5 closely resemble those of hydrated Cu^{2+} sites in zeolites prepared by wet ion exchange reported in the literature.[41−43] It should be noted that no distinct changes are observed in the spectral profile of Cu-containing zeolites prepared from different OSDA-free seed systems. The minor changes might be explained by slight changes in the covalency or coordination symmetry of the copper sites.

EPR spectroscopy was applied to investigate the speciation of Cu^{2+} ions in the current study of Cu-ZSM-5 samples in both hydrated and dehydrated states. Figure 8a displays the EPR spectra of the hydrated Cu-containing ZSM-5 at room temperature. The spectra of all hydrated samples are recorded at room temperature with almost identical features, namely, broad and partly resolved spectra indicative of axially symmetric Cu^{2+} complexes. According to the spectral simulation provided in Figure SI3, they all have a mixture of predominantly rigid species (80% of species A) with the spin Hamiltonian parameters of $g_{xx,yy}$ = 2.076, g_{zz} = 2.360, $A_{xx,yy}$ = 30 MHz, and A_{zz} = 440 MHz, and an additional minor contribution of mobile species (20% of species B) with g_{iso} = 2.145. The relative amount of paramagnetic Cu^{2+} species in the hydrated samples was determined by double integration of the respective EPR spectra and then normalized by the weight of the sample. The information on relative EPR intensities is provided in Table 3 in the order as follows: Cu-ZSM-5_ 3 (3.7) > Cu-ZSM-5_4 (2.4) > Cu-ZSM-5_1 (1.6) > Cu-ZSM-5_2 (1.0). The dehydrated spectrum (Figure 8b) shows more resolved EPR spectra, and three species (species C, D, and E) are included in the spectral simulation, as can be seen in Figure 9. The spectral simulation was based on the spin Hamiltonian parameter obtained from the pulsed EPR approach by Sass and Kevan.[44] The respective weight contribution of each species in the spectra is summarized in Table 4. Both Cu-ZSM-5_1 and Cu-ZSM-5_2 are characterized using species E (g_{zz} = 2.304 and A_{zz} = 525 MHz) as the dominant species with 80% weight, while species C (g_{zz} = 2.369 and A_{zz} = 441 MHz) and species D (g_{zz} = 2.365 and A_{zz} = 470 MHz) are contributed as a minor component of the signal (10% each). In the case of the Cu-ZSM-5_3 and Cu-ZSM-5_4 samples, species E accounted for 65% followed by species D (30%) and a trace amount of species C (5%). The only potentially possible source of marked (Figure 9a,d) carbon radicals in the samples could be due to some disintegration of acetate anion that comes from copper(II) acetate that was utilized for ion exchange. However, the CP/*MAS* ^{13}C *NMR* measurements and XPS analysis did not reveal any carbonates (results not shown).

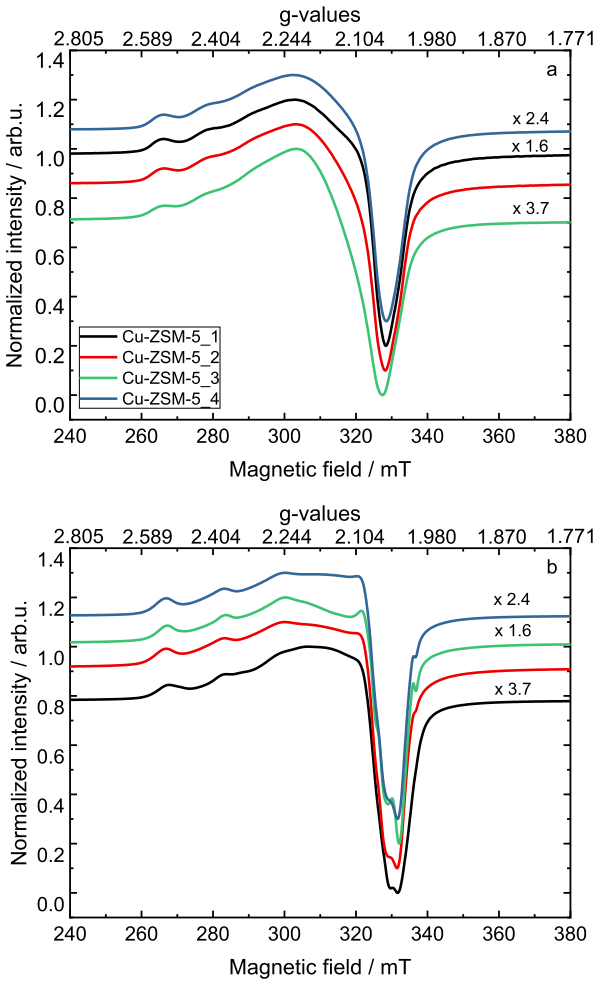

Figure 8. (a) EPR spectra of Cu-containing ZSM-5 recorded at room temperature and (b) EPR spectra of activated samples (activation at 400 °C for 5 h under vacuum) recorded at −196 °C; in (a,b), the sample labels are equal.

At the hydrated state, species B is commonly observed in a multitude of examples for copper-exchanged zeolites as freely tumbled $[Cu(H_2O)_6]^{2+}$ complexes.[44−47] Species A can be attributed to the $[Cu(O_f)_3(H_2O)_3]^{2+}$ species according to the pulse EPR study.[31] The latter might be accommodated at the channel intersection of the MFI framework. The evolution of species upon activation under vacuum (400 °C for 5 h) can be rationalized by the fact that as the temperature increases, water ligands are gradually detached from the Cu^{2+} complex and coordinated to the framework oxygen.[48] The value of g_{zz} is expected to decrease, whereas A_{zz} is expected to increase when the coordination number is lowered successively from the six-coordinated Cu^{2+} to the four-coordinated Cu^{2+}. Species C (g_{zz} = 2.369 and A_{zz} = 441 MHz) exhibits a similar spin Hamiltonian parameter to species A; therefore, it is safe to assume that species C can be attributed to the $[Cu(O_f)_3(H_2O)_3]^{2+}$ species located mainly in the channel intersection. In the case of species D (g_{zz} = 2.365 and A_{zz} = 470 MHz), a slightly higher A_{zz} value than in the case of species C is observed, so we expect that it contains fewer water molecules than species C ($[Cu(O_f)_3(H_2O)_3]^{2+}$). In addition, species E (g_{zz} = 2.304 and A_{zz} = 525 MHz) is expected to exclusively coordinate with oxygen at the zeolite lattices after the removal of all water ligands (i.e., $[Cu(O_f)_4]^{2+}$). It exhibits a square planar Cu^{2+} configuration in line with the spin Hamiltonian parameter obtained from previous literature.[12,44,48] It is interesting to compare the EPR pattern of OSDA-free Cu-ZSM-5 (current work) and Cu-ZSM-5 with OSDA reported by previous literature.[12,13] Taking into account the variability of the n(Si)/n(Al) ratio and the Cu^{2+} content, the EPR spectra for OSDA-free Cu-ZSM-5 samples after activation treatment have significant g and A strains indicative

https://doi.org/10.1021/acsomega.3c03721
ACS Omega 2023, 8, 41107−41119

Table 3. Spin Hamiltonian Parameters Used for Spectral Simulation of Cu-Containing ZSM-5 before and after Activation at 400 °C for 5 h under Vacuum Conditions

sample state	Cu species	$g_{xx,yy}$	g_{zz}	$A_{xx,yy}$/MHz	A_{zz}/MHz	lwpp/mT	assignment
hydrated	A	2.075 ± 0.003	2.360 ± 0.003	30 ± 5	440 ± 5	4.0 ± 0.2	$[Cu(O_f)_3(H_2O)_3]^{2+}$
	B	2.145[a]					$[Cu(H_2O)_6]^{2+}$
activated	C	2.075 ± 0.003	2.369 ± 0.003	30 ± 5	441 ± 5	3.0 ± 0.2	$[Cu(O_f)_3(H_2O)_3]^{2+}$
	D	2.075 ± 0.003	2.320 ± 0.003	30 ± 5	470 ± 5	3.0 ± 0.2	$[Cu(O_f)_m(H_2O)_n]^{2+}, n < 3$
	E	2.075 ± 0.003	2.304 ± 0.003	30 ± 5	525 ± 5	3.0 ± 0.2	$[Cu(O_f)_4]^{2+}$

[a] g_{iso} is an isotropic g-value. g-strain is applied at the perpendicular position within the range of 0.04−0.08. The lwpp is the line width parameter that is adjusted during the simulation.

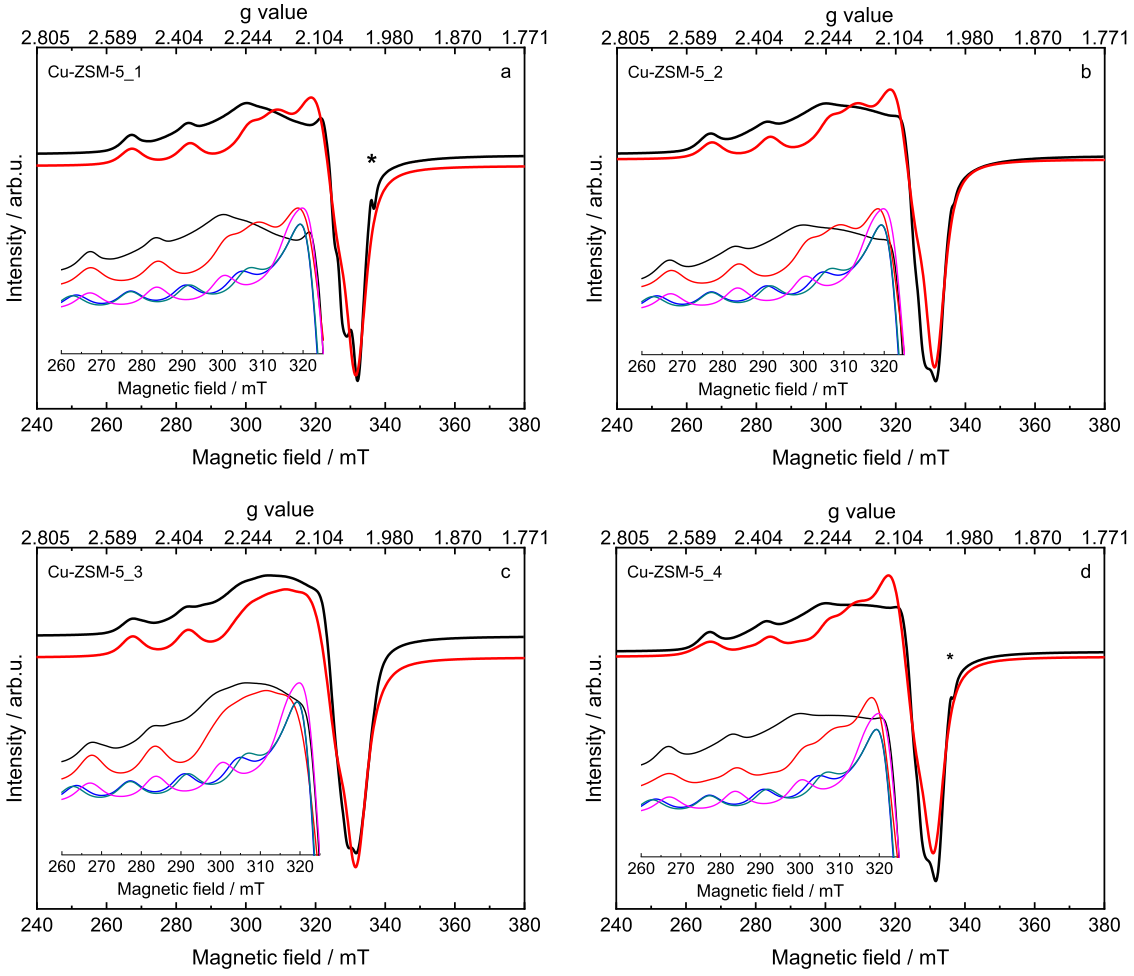

Figure 9. Experimental (black) and simulated (red) EPR spectra of activated Cu-containing ZSM-5 recorded at −196 °C: (a) Cu-ZSM-5_1, (b) Cu-ZSM-5_2, (c) Cu-ZSM-5_3, and (d) Cu-ZSM-5_4. The signal marked with a blue star indicates a residual carbon radical. The inset shows the decomposition of simulated spectra into the contributing subspectra of species C (blue), D (dark cyan), and E (magenta).

Table 4. Composition in Percentage for Different Cu Species in Activated Cu-Containing ZSM-5 Obtained from the Spectral Simulations Using EasySpin[26a]

sample	C/%	D/%	E/%
Cu-ZSM-5_1	10	10	80
Cu-ZSM-5_2	10	10	80
Cu-ZSM-5_3	5	30	65
Cu-ZSM-5_4	5	30	65

[a] The uncertainty of 3% has been estimated during spectral simulation.

of more Cu^{2+} site heterogeneity if compared to the spectra of Cu-ZSM-5 synthesized using OSDA.[49]

The in situ DRIFTS were collected for Cu-ZSM-5_3, Cu-ZSM-5_4, and Cu-ZSM-5−170 under a NH_3 flow. Cu-ZSM-5−170 represents the material prepared in the conventional way in the presence of OSDA and was fully characterized in our previous studies.[13] As shown in Figure 10, the band at 3607 cm^{-1} is attributed to the protonated OH groups (mainly Si−OH−Al) consumed by NH_3,[50] while the bands located below 3400 cm^{-1} (i.e., 3358 and 3278 cm^{-1}) are the result of N−H vibrations of ammonia. Meanwhile, the band at 1459 cm^{-1} was observed, referring to the NH_4^+ on Brønsted acid sites.[51,52] The negative band at 3659 cm^{-1} is ascribed to the vibration of Cu−OH groups coordinated by NH_3.[52] The bands at 3184, 1618, 1293, and 1190 cm^{-1} are related to the NH_3

https://doi.org/10.1021/acsomega.3c03721
ACS Omega 2023, 8, 41107−41119

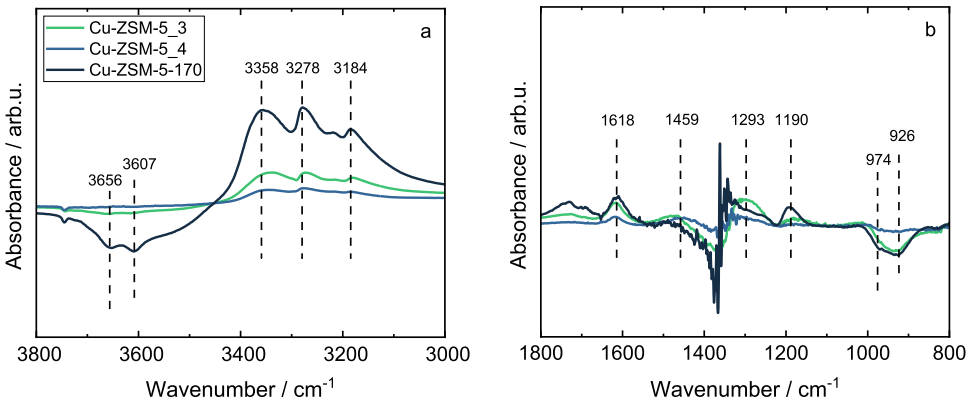

Figure 10. In situ DRIFTS spectra of Cu-ZSM-5_3, Cu-ZSM-5_4, and Cu-ZSM-5−170 collected at 150 °C; reaction conditions: m_K = 0.1 g, F_{TOT} = 120 mL min^{-1}, $c(NH_3)$ = 575 ppm; (a) high wavenumber in the range of 3000−3800 cm^{-1} and (b) low wavenumber in the range of 800−1800 cm^{-1}; in (a,b), the sample labels are equal.

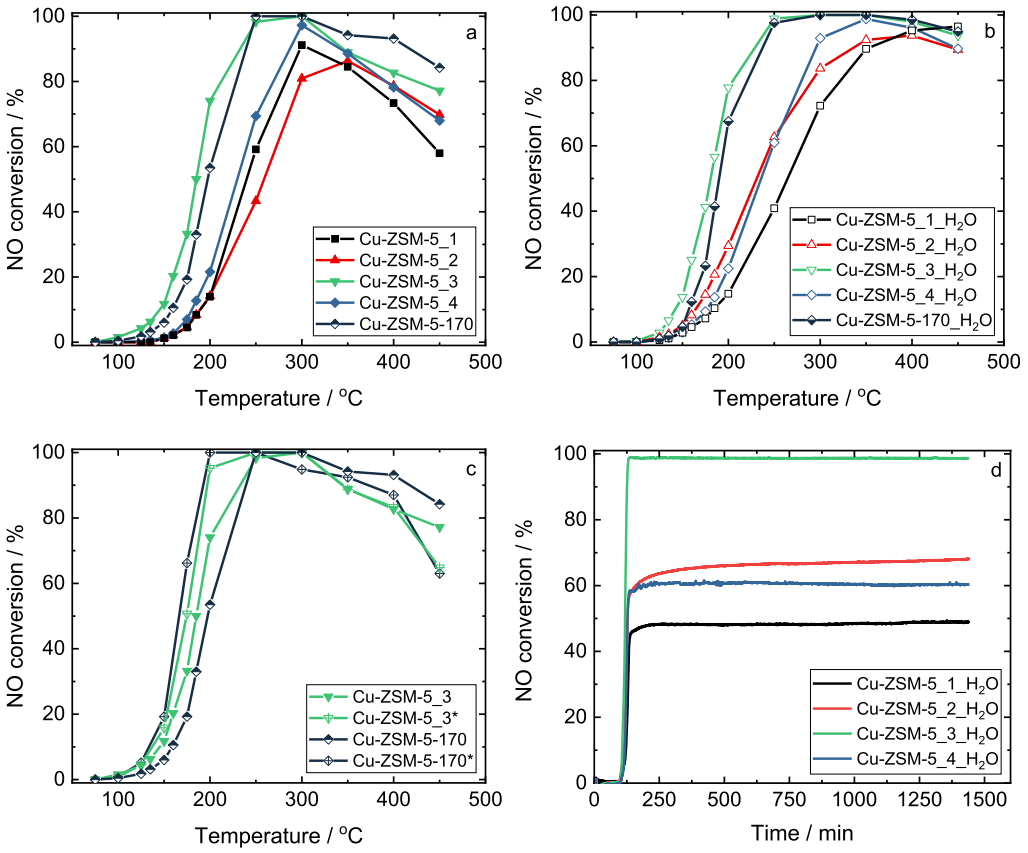

Figure 11. Results of catalytic studies: (a) NO conversion, reaction conditions: m_K = 0.1 g, F_{TOT} = 120 mL min^{-1}, c(NO) = 500 ppm, $c(NH_3)$ = 575 ppm, $c(O_2)$ = 4 vol %, He balance, GHSV = 30,000 h^{-1}; (b) NO conversion in the presence of H_2O ($c(H_2O)$ = 5 vol %); (c) reaction conditions: *m_K = 0.1 g, F_{TOT} = 120 mL min^{-1}, c(NO) = 1000 ppm, $c(NH_3)$ = 1000 ppm, $c(O_2)$ = 10 vol %, He balance, GHSV = 30 000 h^{-1} (without * reaction conditions as in panel a), and (d) time-on-stream stability tests at 250 °C in the presence of H_2O ($c(H_2O)$ = 5 vol %), reaction conditions equal to (b).

adsorbed on the Cu^{2+} sites, which is referred to the Lewis acid sites.[53] It can be observed that the absorbance intensity of Cu-ZSM-5−170 is higher than those for the other two zeolites in terms of both Brønsted and Lewis sites, indicating a higher number of catalytic acid sites. The presence of Cu cations leads to local framework perturbation, which is examined by analyzing the T−O−T vibration region.[54] In the low wavenumber range, two negative bands at 974 and 926 cm^{-1} are present, corresponding to a weakened perturbation of zeolite T−O−T asymmetric vibrations by $[Cu(OH)]^+$ and Cu^{2+}, respectively.[55] For the Cu-ZSM-5_3 sample, there are no significant negative bands in these positions, indicating a lower content of Cu species at the exchange positions compared to Cu-ZSM-170.

Figure 11 shows the NO conversion in NH_3−SCR-DeNO$_x$ without H_2O (panel a) and in the presence of H_2O in the feed (panel b), while Table 5 provides the activation energy of the Cu-containing ZSM-5 and the TOF in the same temperature range. Among the studied materials, only Cu-ZSM-5_3 reveals more than 80% NO conversion between 250 and 400 °C. Cu-

https://doi.org/10.1021/acsomega.3c03721
ACS Omega 2023, 8, 41107−41119

Table 5. Activation Energy of the Cu-Containing ZSM-5 in NH_3−SCR-DeNO$_x$ without H_2O and in the Presence of H_2O (*) and the TOF in the Same Temperature Range

sample	E_a/kJ mol^{-1}	TOF × 10^{-3}/s^{-1}
Cu-ZSM-5_1	83 (150−175°C)/	0.02−0.07/
	90 (125−150°C)*	0.01−0.04*
Cu-ZSM-5_2	82 (150−175°C)/	0.02−0.07/
	71 (125−150°C)*	0.02−0.08*
Cu-ZSM-5_3	51 (100−135°C)/	0.02−0.10/
	107 (100−135°C)*	0.01−0.10*
Cu-ZSM-5_4	75 (125−150°C)/	0.01−0.02/*
	79 (125−150°C)*	0.01−0.05
Cu-ZSM-5−170	71 (100−135°C)/	0.02−0.03/
	88 (125−150°C)*	0.01−0.05*

ZSM-5_4, based on the ZSM-5 seeds prepared at 170 °C, showed significantly lower activity, while both samples based on silicalite-1 possess the lowest activity. The activity of the materials significantly dropped above 300 °C without water due to a side reaction of ammonia oxidation.[56] Thus, in the presence of H_2O in the feed, the activity was improved for all samples due to competitive adsorption between NH_3 and H_2O. All catalysts maintained their stability for 24 h at 250 °C during the time-on-stream in the presence of 5 vol % H_2O (panel d). The NO conversions achieved after 24 h were consistent with the previously measured NO conversion during the NH_3−SCR-DeNO$_x$ experiments with water (Figure 11b). Again, at 250 °C, only the sample Cu-ZSM-5_3 shows a NO conversion of more than 99%. For all other samples, the NO conversion varies between 45 and 70% (Figure 11d). The outcome stresses the importance of the crystalline structure, i.e., long-range order, of the material in the catalytic systems. Probably, the rigid confinement stabilizes the Cu species. The Cu-ZSM-5_3 sample preserves still its crystalline structure after the modification at 500 °C for 5 h in the presence of 10 vol % of H_2O (data not shown here). Amorphous materials do not possess long-range order, and there is a plethora of possible Cu coordinations/species in such an environment. The materials based on the ZSM-5 seeds revealed high activity in NH_3−SCR-DeNO$_x$ under two different feed conditions (Figure 11a versus Figure 11c, Table 5), while NO conversion over Cu-ZSM-5_3 is comparable to the activity achieved before by the materials prepared in the conventional way in the presence of OSDAs.[13] Thus, this research provides guidelines for designing materials efficiently in NH_3−SCR-DeNO$_x$ over OSDA-free and environment-friendly catalysts.

4. CONCLUSIONS

These studies compared the activities of Cu-containing ZSM-5 prepared from different OSDA-free seed systems. Thus, silicalite-1 (as a 12 vol % suspension applied for the sample called Cu-ZSM-5_1; as a dry, noncalcined powder—Cu-ZSM-5_2) and ZSM-5 (in the form of a dry, noncalcined powder prepared at 100 °C applied for the sample named Cu-ZSM-5_3; and prepared at 170 °C — Cu-ZSM-5_4) were used as seeds. The materials based on the ZSM-5 seeds revealed high activity in NH_3−SCR-DeNO$_x$, which is comparable to the material prepared in a conventional way in the presence of OSDA. Thus, Cu nanoparticles evenly distributed in the crystallites and amorphous particles of Cu-ZSM-5_3 are the main active sites in NH_3−SCR-DeNO$_x$. Otherwise, the dominant speciation form of copper is isolated Cu^{2+} cations in Cu-ZSM-5−170.

■ ASSOCIATED CONTENT

Supporting Information

The Supporting Information is available free of charge at https://pubs.acs.org/doi/10.1021/acsomega.3c03721.

Additional data for XRD, NMR, and EPR studies for Cu-containing ZSM-5 samples (PDF)

■ AUTHOR INFORMATION

Corresponding Author

Magdalena Jabłońska − *Institute of Chemical Technology, Universität Leipzig, 04103 Leipzig, Germany;* orcid.org/0000-0002-7868-1067; Email: magdalena.jablonska@uni-leipzig.de

Authors

Ana Palčić − *Laboratory for the Synthesis of New Materials, Division of Materials Chemistry, Ruđer Bošković Institute, 10000 Zagreb, Croatia;* orcid.org/0000-0002-1092-4739

Muhammad Fernadi Lukman − *Felix Bloch Institute for Solid State Physics, Universität Leipzig, 04103 Leipzig, Germany*

Anna Wach − *PSI, Forschungsstrasse 111, 5232 Villigen, Switzerland;* Present Address: National Synchrotron Radiation Centre SOLARIS, Jagiellonian University, Krakow, Poland; orcid.org/0000-0003-3112-2759

Marko Bertmer − *Felix Bloch Institute for Solid State Physics, Universität Leipzig, 04103 Leipzig, Germany;* orcid.org/0000-0002-3208-7927

David Poppitz − *Institute of Chemical Technology, Universität Leipzig, 04103 Leipzig, Germany*

Reinhard Denecke − *Wilhelm-Ostwald-Institute for Physical and Theoretical Chemistry, Universität Leipzig, D-04103 Leipzig, Germany*

Xiaochao Wu − *Institute of Inorganic Chemistry, RWTH Aachen University, 52074 Aachen, Germany;* orcid.org/0000-0003-4374-9743

Ulrich Simon − *Institute of Inorganic Chemistry, RWTH Aachen University, 52074 Aachen, Germany;* orcid.org/0000-0002-6118-0573

Andreas Pöppl − *Felix Bloch Institute for Solid State Physics, Universität Leipzig, 04103 Leipzig, Germany*

Roger Gläser − *Institute of Chemical Technology, Universität Leipzig, 04103 Leipzig, Germany;* orcid.org/0000-0002-8134-4280

Complete contact information is available at: https://pubs.acs.org/10.1021/acsomega.3c03721

Author Contributions

M.J.: conceptualization, methodology, investigation, data curation, writing—original draft, writing—review and editing, and supervision. A.P.: investigation, data curation, and writing—review and editing. M.F.L.: investigation, data curation, and writing—review and editing. A.W.: investigation, data curation, and writing—review and editing. M.B.: investigation, data curation, and writing—review and editing. D.P.: investigation and data curation. R.D.: investigation, data curation, and review. X.W.: investigation, data curation, and writing—review and editing. U.S.: review. A.P.: review. R.G.: review.

https://doi.org/10.1021/acsomega.3c03721
ACS Omega 2023, 8, 41107−41119

Notes

The authors declare no competing financial interest.

■ ACKNOWLEDGMENTS

M.J. acknowledges a DFG Research Grant JA 2998/2-1. A.P. acknowledges the funding of the Croatian Science Foundation under the project UIP-2019-04-4977. M.F.L. acknowledges a DFG Research Grant (Project ID 443871192, GRK 2721: Hydrogen Isotopes 1,2,3). The authors acknowledge the Swiss Light Source (SLS) for providing access to the SuperXAS (X10DA) beamline for ex situ XAS measurements (proposal no. 20222315). X.W. and U.S. gratefully acknowledge financial support from DFG, under Germany's Excellence Strategy—Cluster of Excellence 2186 "The Fuel Science Center" (ID: 390919832).

■ REFERENCES

(1) Nagy, J. B.; Bodart, P.; Hannus, I.; Kiricsi, I. *Synthesis and Use of Zeolitic Microporous Materials*; DecaGen: Szeged-Szõreg, 1998.
(2) Zhang, Q.; Yu, J.; Corma, A. Applications of Zeolites to C1 Chemistry: Recent Advances, Challenges, and Opportunities. *Adv. Mater.* **2020**, *32*, 2002927.
(3) Palčić, A.; Valtchev, V. Synthesis and Application of (nano) Zeolites, *Reference Module in Chemistry, Molecular Sciences and Chemical Engineering*; U.S. Department of Energy, 2021.
(4) Tang, L.; Haw, K.-G.; He, P.; Fang, Q.; Qiu, S.; Valtchev, V. Synthesis of Zeolite SSZ-24 Using a Catalytic Amount of SSZ-13 Seeds. *Inorg. Chem. Front.* **2019**, *6*, 3097−3103.
(5) Majano, G.; Darwiche, A.; Mintova, S.; Valtchev, V. Seed-Induced Crystallization of Nanosized Na-ZSM-5 Crystals. *Ind. Eng. Chem.* **2009**, *48*, 7084−7091.
(6) Cheng, Y.; Wang, L.-J.; Li, J.-S.; Yang, Y.-C.; Sun, X.-Y. Preparation and Characterization of Nanosized ZSM-5 Zeolites in the Absence of Organic Template. *Mater. Lett.* **2005**, *59*, 3427−3430.
(7) Razavian, M.; Fatemi, S.; Komasi, M. Seed-Assisted OSDA-Free Synthesis of ZSM-5 Zeolite and Its Application in Dehydrogenation of Propane. *Mater. Res. Bull.* **2015**, *65*, 253−259.
(8) Shen, K.; Wang, N.; Chen, X.; Chen, Z.; Li, Y.; Chen, J.; Qian, W.; Wei, F. Seed-Induced and Additive-Free Synthesis of Oriented Nanorod-Assembled Meso/Macroporous Zeolites: Toward Efficient and Cost-Effective Catalysts for the MTA Reaction. *Catal. Sci. Technol.* **2017**, *7*, 5143−5153.
(9) Dai, C.; Li, J.; Zhang, A.; Nie, C.; Song, C.; Guo, X. Precise Control of the Size of Zeolite B-ZSM-5 Based on Seed Surface Crystallization. *RSC Adv.* **2017**, *7*, 37915−37922.
(10) Chen, H.; Wang, Y.; Meng, F.; Sun, C.; Li, H.; Wang, Z.; Gao, F.; Wang, X.; Wang, S. Aggregates of Superfine ZSM-5 Crystals: The Effect of NaOH on the Catalytic Performance of Methanol to Propylene Reaction. *Microporous Mesoporous Mater.* **2017**, *244*, 301−309.
(11) Tarach, K. A.; Jabłońska, M.; Pyra, K.; Liebau, M.; Reiprich, B.; Gläser, R.; Góra-Marek, K. Effect of Zeolite Topology on NH_3-SCR Activity and Stability of Cu-Exchanged Zeolites. *Appl. Catal., B* **2021**, *284*, 119752.
(12) Jabłońska, M.; Góra-Marek, K.; Grilc, M.; Bruzzese, P. C.; Poppitz, D.; Pyra, K.; Liebau, M.; Pöppl, A.; Likozar, B.; Gläser, R. Effect of Textural Properties and Presence of Co-Cation on NH_3-SCR Activity of Cu-Exchanged ZSM-5. *Catalysts* **2021**, *11*, 843.
(13) Jabłońska, M.; Góra-Marek, K.; Bruzzese, P. C.; Palčić, A.; Pyra, K.; Tarach, K.; Bertmer, M.; Poppitz, D.; Pöppl, A.; Gläser, R. Influence of Framework n(Si)/n(Al) Ratio on the Nature of Cu Species in Cu-ZSM-5 for NH_3-SCR-DeNO_x. *ChemCatChem* **2022**, *14*, No. e202200627.
(14) Tomita, J.; Elangovan, S. P.; Itabashi, K.; Chokkalingam, A.; Fujinuma, H.; Hao, Z.; Kanno, A.; Hayashi, K.; Iyoki, K.; Wakihara, T.; Okubo, T. OSDA-Free Synthesis of Zeolite Beta: Broadening the Methodology for a Successful Use of the Product as a Seed. *Adv. Powder Technol.* **2022**, *33* (9), 103741.
(15) Jain, R.; Rimer, J. D. Seed-Assisted Zeolite Synthesis: The Impact of Seeding Conditions and Interzeolite Transformations on Crystal Structure and Morphology. *Microporous Mesoporous Mater.* **2020**, *300*, 110174.
(16) Kwak, J. H.; Tran, D.; Burton, S. D.; Szanyi, J.; Lee, J. H.; Peden, C. H. F. Effects of Hydrothermal Aging on NH_3-SCR Reaction over Cu/Zeolites. *J. Catal.* **2012**, *287* (3), 203−209.
(17) Schmidt, J. E.; Oord, R.; Guo, W.; Poplawsky, J. D.; Weckhuysen, B. M. Nanoscale Tomography Reveals the Deactivation of Automotive Copper-Exchanged Zeolite Catalysts. *Nat. Commun.* **2017**, *8* (1), 1666.
(18) Valtchev, V. Preparation of Regular Macroporous Structures Built of Intergrown Silicalite-1 Nanocrystals. *J. Mater. Chem.* **2002**, *12*, 1914−1918.
(19) Palčić, A.; Ordomsky, V. V.; Qin, Z.; Georgieva, V.; Valtchev, V. Tuning Zeolite Properties for Highly Efficient Synthesis of Propylene from Methanol. *Chem.—Eur. J.* **2018**, *24*, 13136.
(20) Zhang, H.; Ma, Y.; Song, K.; Zhang, Y.; Tang, Y. Nano-Crystallite Oriented Self-Assembled ZSM-5 Zeolite and Its LDPE Cracking Properties: Effects of Accessibility and Strength of Acid Sites. *J. Catal.* **2013**, *302*, 115−125.
(21) Xue, T.; Chen, L.; Wang, Y. M.; He, M.-Y. Seed-Induced Synthesis of Mesoporous ZSM-5 Aggregates Using Tetrapropylammonium Hydroxide as Single Template. *Microporous Mesoporous Mater.* **2012**, *156*, 97−105.
(22) Wu, G.; Wu, W.; Wang, X.; Zan, W.; Wang, W.; Li, C. H. Nanosized ZSM-5 Zeolites: Seed-Induced Synthesis and the Relation between the Physicochemical Properties and the Catalytic Performance in the Alkylation of Naphthalene. *Microporous Mesoporous Mater.* **2013**, *180*, 187−195.
(23) https://www.unifit-software.de/ (accessed May 26, 2023).
(24) Clark, A. H.; Imbao, J.; Frahm, R.; Nachtegaal, M. ProQEXAFS: A Highly Optimized Parallelized Rapid Processing Software for QEXAFS Data. *J. Synchrotron Radiat.* **2020**, *27*, 551−557.
(25) Ravel, B.; Newville, M. Athena, Artemis, Hephaestus: Data Analysis for X-Ray Absorption Spectroscopy Using IFEFFIT. *J. Synchrotron Radiat.* **2005**, *12*, 537−541.
(26) Stoll, S.; Schweiger, A. EasySpin, A Comprehensive Software Package for Spectral Simulation and Analysis in EPR. *J. Magn. Reson.* **2006**, *178*, 42−55.
(27) Massiot, D.; Fayon, F.; Capron, M.; King, I.; Le Calvé, S.; Alonso, B.; Durand, J.-O.; Bujoli, B.; Gan, Z.; Hoatson, G. Modelling One-and Two-Dimensional Solid-State NMR Spectra. *Magn. Reson. Chem.* **2002**, *40*, 70−76.
(28) Liu, J.; Yu, F.; Liu, J.; Cui, L.; Zhao, Z.; Wei, Y.; Sun, Q. Synthesis and Kinetics Investigation of Meso-Microporous Cu-SAPO-34 Catalysts for the Selective Catalytic Reduction of NO with Ammonia. *J. Environ. Sci.* **2016**, *48*, 45−58.
(29) Bhadra, B. N.; Song, J. Y.; Khan, N. A.; Jun, J. W.; Kim, T.-W.; Kim, C.-U.; Jhung, S. H. Conversion of Ethylene into Propylene with the Siliceous SSZ-13 Zeolite Prepared without an Organic Structure-Directing Agent. *J. Catal.* **2018**, *365*, 94−104.
(30) Kaneko, K.; Otsuka, H. New IUPAC Recommendation and Characterization of Nanoporous Materials with Physical Adsorption. *Acc. Mater. Surf. Res.* **2020**, *5*, 25−32.
(31) Palčić, A.; Moldovan, S.; El Siblani, H.; Vicente, A.; Valtchev, V. Defect Sites in Zeolites: Origin and Healing. *Adv. Sci.* **2022**, *9* (4), 2104414.
(32) Rodríguez-González, L.; Hermes, F.; Bertmer, M.; Rodríguez-Castellón, E.; Jiménez-López, A.; Simon, U. The Acid Properties of H-ZSM-5 as Studied by NH_3-TPD and 27Al-MAS-NMR Spectroscopy. *Appl. Catal., A* **2007**, *328*, 174−182.
(33) Yashnik, S.; Ismagilov, Z. Cu-Substituted ZSM-5 Catalyst: Controlling of DeNO_x Reactivity via Ion-Exchange Mode with Copper-Ammonia Solution. *Appl. Catal., B* **2015**, *170−171*, 241−254.

https://doi.org/10.1021/acsomega.3c03721
ACS Omega 2023, 8, 41107−41119

(34) Vennestrøm, P. N. R.; Janssens, T. V. W.; Kustov, A.; Grill, M.; Puig-Molina, A.; Lundegaard, L. F.; Tiruvalam, R. R.; Concepción, P.; Corma, A. Influence of Lattice Stability on Hydrothermal Deactivation of Cu-ZSM-5 and Cu-IM-5 Zeolites for Selective Catalytic Reduction of NO_x by NH_3. *J. Catal.* **2014**, *309*, 477−490.
(35) De La Torre, U.; Pereda-Ayo, B.; Romero-Sáez, M.; Aranzabal, A.; González-Marcos, M. P.; González-Marcos, J. A.; González-Velasco, J. R. Screening of Fe-Cu-Zeolites Prepared by Different Methodology for Application in NSR-SCR Combined $DeNO_x$ Systems. *Top. Catal.* **2013**, *56*, 215−221.
(36) Montini, T.; Hickey, N.; Fornasiero, P.; Graziani, M.; Bañares, M. A.; Martinez-Huerta, M. V.; Alessandri, I.; Depero, L. E. Variations in the Extent of Pyrochlore-Type Cation Ordering in $Ce_2Zr_2O_8$: A t '-κ Pathway to Low-Temperature Reduction. *Chem. Mater.* **2005**, *17*, 1157−1166.
(37) De Groot, F.; Vankó, G.; Glatzel, P. The 1s X-Ray Absorption Pre-Edge Structures in Transition Metal Oxides. *J. Phys.: Condens. Matter* **2009**, *21*, 104207.
(38) Suharbiansah, S.; Lukman, M. F.; Nannuzzi, C.; Wach, A.; Góra-Marek, K.; Liebau, M.; Palčić, A.; Pöppl, A.; Berlier, G.; Bordiga, S.; Gläser, R.; Jabłońska, M. Effect of the Preparation Method on the Catalytic Properties of Copper-Containing Zeolite Y Applied for NH_3-SCR-$DeNO_x$. *Catal. Sci. Technol.* **2023**, *13*, 3804−3817.
(39) Sano, M.; Komorita, S.; Yamatera, H. XANES Spectra of Copper (II) Complexes: Correlation of the Intensity of the 1s. Fwdarw. 3d Transition and the Shape of the Complex. *Inorg. Chem.* **1992**, *31*, 459−463.
(40) Westre, T. E.; Kennepohl, P.; DeWitt, J. G.; Hedman, B.; Hodgson, K. O.; Solomon, E. I. A Multiplet Analysis of Fe K-Edge 1s→ 3d Pre-Edge Features of Iron Complexes. *J. Am. Chem. Soc.* **1997**, *119*, 6297−6314.
(41) Alayon, E. M. C.; Nachtegaal, M.; Bodi, A.; van Bokhoven, J. A. Reaction Conditions of Methane-to-Methanol Conversion Affect the Structure of Active Copper Sites. *ACS Catal.* **2014**, *4*, 16−22.
(42) Giordanino, F.; Borfecchia, E.; Lomachenko, K. A.; Lazzarini, A.; Agostini, G.; Gallo, E.; Soldatov, A. V.; Beato, P.; Bordiga, S.; Lamberti, C. Interaction of NH_3 with Cu-SSZ-13 Catalyst: A Complementary FTIR, XANES, and XES Study. *J. Phys. Chem. Lett.* **2014**, *5*, 1552−1559.
(43) Wang, H.; Jia, J.; Liu, S.; Chen, H.; Wei, Y.; Wang, Z.; Zheng, L.; Wang, Z.; Zhang, R. Highly Efficient NO Abatement over Cu-ZSM-5 with Special Nanosheet Features. *Environ. Sci. Technol.* **2021**, *55*, 5422−5434.
(44) Sass, C. E.; Kevan, L. Electron Spin Echo Modulation and Electron Spin Resonance Studies of Cupric Ions in H-ZSM-5, Na-ZSM-5, K-ZSM-5, and CA-ZSM-5 Zeolites: Analysis of Carbon-13 Electron Spin Echo Modulation. *J. Phys. Chem.* **1988**, *92*, 5192−5196.
(45) Godiksen, A.; Vennestrøm, P. N. R.; Rasmussen, S. B.; Mossin, S. Identification and Quantification of Copper Sites in Zeolites by Electron Paramagnetic Resonance Spectroscopy. *Top. Catal.* **2017**, *60*, 13−29.
(46) Zamadics, M.; Chen, X.; Kevan, L. Solid-State Ion Exchange in H-SAPO-34: Electron Spin Resonance and Electron Spin Echo Modulation Studies of Copper (II) Location and Adsorbate Interaction. *J. Phys. Chem.* **1992**, *96* (13), 5488−5491.
(47) Yu, J. S.; Kevan, L. Temperature Dependence of Copper (II) Migration and Formation of New Copper (II) Species during Catalytic Propylene Oxidation on Copper (II)-Exchanged Y Zeolite and Comparison with X Zeolite. *J. Phys. Chem.* **1990**, *94*, 7612−7620.
(48) Occhiuzzi, M.; Fierro, G.; Ferraris, G.; Moretti, G. Unusual Complete Reduction of Cu^{2+} Species in Cu-ZSM-5 Zeolites under Vacuum Treatment at High Temperature. *Chem. Mater.* **2012**, *24*, 2022−2031.
(49) Carl, P. J.; Larsen, S. C. EPR Study of Copper-Exchanged Zeolites: Effects of Correlated g-and A-strain, Si/Al Ratio, and Parent Zeolite. *J. Phys. Chem. B* **2000**, *104*, 6568−6575.
(50) Chen, Z.; Bian, C.; Guo, Y.; Pang, L.; Li, T. Efficient Strategy to Regenerate Phosphorus-Poisoned Cu-SSZ-13 Catalysts for the NH_3-SCR of NO_x: The Deactivation and Promotion Mechanism of Phosphorus. *ACS Catal.* **2021**, *11*, 12963−12976.
(51) Rizzotto, V.; Chen, D.; Tabak, B. M.; Yang, J.-Y.; Ye, D.; Simon, U.; Chen, P. Spectroscopic Identification and Catalytic Relevance of NH_4^+ Intermediates in Selective NO_x Reduction over Cu-SSZ-13 Zeolites. *Chemosphere* **2020**, *250*, 126272.
(52) Xue, H.; Guo, X.; Meng, T.; Guo, Q.; Mao, D.; Wang, S. Cu-ZSM-5 Catalyst Impregnated with Mn-Co Oxide for the Selected Catalytic Reduction of NO: Physicochemical Property-Catalytic Activity Relationship and in Situ DRIFTS Study for the Reaction Mechanism. *ACS Catal.* **2021**, *11*, 7702−7718.
(53) Lezcano-Gonzalez, I.; Deka, U.; Arstad, B.; Van Yperen-De Deyne, A.; Hemelsoet, K.; Waroquier, M.; Van Speybroeck, V.; Weckhuysen, B. M.; Beale, A. M. Determining the Storage, Availability and Reactivity of NH_3 within Cu-Chabazite-Based Ammonia Selective Catalytic Reduction Systems. *Phys. Chem. Chem. Phys.* **2014**, *16*, 1639−1650.
(54) Han, J.; Wang, A.; Isapour, G.; Härelind, H.; Skoglundh, M.; Creaser, D.; Olsson, L. N_2O Formation during NH_3-SCR over Different Zeolite Frameworks: Effect of Framework Structure, Copper Species, and Water. *Ind. Eng. Chem.* **2021**, *60* (49), 17826−17839.
(55) Wang, A.; Arora, P.; Bernin, D.; Kumar, A.; Kamasamudram, K.; Olsson, L. Investigation of the Robust Hydrothermal Stability of Cu/LTA for NH_3-SCR Reaction. *Appl. Catal., B* **2019**, *246*, 242−253.
(56) Rizzotto, V.; Bajić, S.; Formenti, D.; Wu, X.; Sauerbeck, S.; Werner, J.; Weirich, T. E.; Janke, T.; Mauermann, P.; Pischinger, S.; Palkovits, R.; Simon, U. Comparison of Industrial and Lab-Scale Ion Exchange for the $DeNO_x$-SCR Performance of Cu Chabazites: A Case Study. *Catalysts* **2022**, *12*, 880.

https://doi.org/10.1021/acsomega.3c03721
ACS Omega 2023, 8, 41107−41119